ISSN: 2096-3246
Volume 58, Issue 01, 2026

BATCH SEPARATION AND THERMAL KINETIC STUDIES OF NOVEL POLYMER

Akshay A. Akare[1], W. B. Gurnule[2*] and D. M. Chafle[1]
[1]Department of Chemistry Taywade College, Mahadula, Koradi, Nagpur- 441111 India.
[*2]Department of Chemistry Kamla Nehru Mahavidyalaya, Nagpur- 440024 India.
E-mail: akshayakare10@gmail.com, wbgurnule@gmail.com, dmchafle@gmail.com
Orchid:0009-0002-5793-857X

Abstract

A novel polymer was synthesized through the condensation of 2, 4-dihydroxybenzoic acid with acrylamide and formaldehyde. The polymer was comprehensively characterized by elemental analysis, physico-chemical methods, and spectrometry such as Ultraviolet Visible spectroscopy, Infrared spectroscopy and Proton Nuclear Magnetic Resonance. Semi-crystalline nature of polymer was exported using electron Beam microscopy. GPC (gel permeation chromatography) was implemented to figure out the molecular weight of the polymer. To assess its metal adsorption capabilities, a batch separation performance was used for the selective extraction of toxic traces metallic cation such as Co^{2+}, Cd^{2+}, and Pb^{2+}. Experimental outcomes indicated that the synthesized polymer possesses a highly permeable and major surface area, contributing to its enhanced metal ion uptake. When differentiate with marketable available phenolic and polystyrene resins, the polymer demonstrated superior adsorption performance. By employing thermogravimetric analysis (TGA), the polymer's thermal stability has been assessed. Detailed thermal decomposition behavior was studied, and kinetic parameters were evaluated using both the Freeman–Carroll and Sharp–Wentworth methods. The consistency between the results from both methods confirmed the reliability of the thermal analysis.

Keywords: Polymer, Morphology, Ion-exchange, Toxic metals, Thermodynamic property.

Introduction

Polymer science has rapidly evolved, drawing global attention due to the versatile applications of polymer materials due to which industries such as mining, refining, battery manufacturing, paint production, chemical production, dye manufacturing, and pharmaceuticals have grown significantly worldwide. Many of these industries contribute to widespread environmental pollution, particularly through the release of toxic metals like (Co^{2+}, Cd^{2+}, Pb^{2+}) into the soil and aquatic systems. These toxic metals ions are highly hazardous and posing serious risks to human health and other living organisms. Living systems near these industries often absorb heavy metal toxins in various forms, leading to health risks and hazards, including skin, lung, and liver cancer [1]. Addressing the current environmental challenge of removing toxic metal contaminants from wastewater and industrial effluents involves various conventional methods, including precipitate formation, electrochemistry, microfiltration, biotrement and demineralization. Among these, cation exchange examination proves highly effective due to its enhanced adsorption capacity, strong selectivity, and excellent reusability [2-4].

Copolymers and their metal-coordinated polymer systems exhibit excellent thermal stability, remarkable come up with to the development of advanced polymeric compounds [5]. Gurnule and co-researchers studied the thermal degradation behaviour as concerns copolymer prepared using

monomeric material including 1, 5-diaminonaphthalene with 2-hydroxy-4-methoxybenzophenone and formaldehyde was found thermally more stable [6]. The copolymer was produced through polymerization, employing like 2, 4-dihydroxybenzoic acid with phenylhydrazine and formaldehyde in a 3:1:5 molar ratio. An acid catalyst facilitated the polymerization process [7-9].

The capacity of the synthesized copolymer to occupy metal ions was examined using the batch equilibration technique, considering different metal ions across varying concentrations. A comparative study was performed between strong anion exchange poly styrene, ethylene glycol dimethacrylate vinylbenzyl chlorideand hypercrosslinked strong anion exchange poly copolymerizing 2-hydroxyethyl methacrylate ethylene glycol dimethacrylate and vinylbenzyl chloride [10].

Substituted resorcinol, biuret, and formaldehyde shows antimicrobial properties, and cation exchange characteristics of a copolymer compound [11]. A different copolymer resin was developed from diaminobenzoic acid with 2-hydroxybenecarboxylic acid and methanal, and its metal-binding deionization capabilities were examined through the batch equilibrium method. The polymer showed major affinity for ferrous, copper, and nickel ions over zinc, cobalt, and lead ions. [12]. Semicarbazide with 2-hydroxybenzoic acid and formaldehyde copolymer in existence of catalyst and work on its cation exchange distinguishing feature for copper, zinc, nickel, cobalt and lead ions which shows remarkable ion exchange properties [13-14].

Thermal stability and kinetic characteristics of the synthesized resins were examined using thermogravimetric analysis (TGA) to investigate their degradation mechanisms [15–16]. The analysis showed that higher heating rates result in an accelerated thermal decomposition process.

The synthesized p-xylylane-Aza222 polymer exhibited higher efficiency and selectivity in the recovery of mercury ions, which follows a physisorption mechanism [17]. The study also investigated the recovery of Hg^{2+} ions using a polyaniline and polystyrene composite through a radiotracer technique, revealing that an increase in temperature enhances metal sorption. Furthermore, at temperatures between 25°C and 70°C hexavalent chromium (VI) ions were effectively removed using a PGME copolymer through the batch equilibrium technique.

The thermal degradation investigation discover 2-H4-MBP1, 5-DAPF copolymer which exhibit extensively stability under at temperature [18]. Growing interest in copolymer characteristics is driven by their influence on thermal stability and functional adaptability. Numerous researchers have focused on improving high-temperature thermal stability by altering the monomer composition during the polymerization process [20–21]. Das investigated a copolymer further it was compared with its composite which show remarkable thermal strength [22]. Bisen and co-workers studied thermal degradation thermodynamic and kinetic framework which show remarkable thermal stable copolymer [23].

Copolymers are widely used in adherent, covering, photoelectric cells [24], and junction transistor [25] because they offer a balanced combination of thermal stability and manufacturing flexibility. They have also been investigated for diverse applications, including use as activators, ion exchangers, catalysts, and materials with high thermal resistance [26-27].

In the current investigation, a novel polymer was synthesized using the condensation method engaging 2, 4-dihydroxybenzoic acid, acrylamide, and formaldehyde. The molecular weight of the

resulting polymers exist examined through gel penetration chromatography. The synthesized polymer were thoroughly characterized using physico-chemical, elemental, and spectral analyses, along with SEM and TGA techniques. Ion-exchange behaviour was studied via the batch separation method. Additionally, the thermostablity and decomposition kinetics of the polymer were assessed using TGA. A comprehensive comparative study, focusing on metal ion removal efficiency and thermal properties, was also carried out between the synthesized polymer and commercially available resins.

Experimental

Materials

Analytical grade reagents were used throughout the study without any additional treatment. 2,4-Dihydroxybenzoic acid, along with acrylamide and formaldehyde (procured from SD Fine), as well as metal nitrates and chlorides of Pb^{2+}, Cd^{2+}, Hg^{2+}, and Co^{2+}, were sourced from Central Scientific Company, Nagpur, and used without further purification. Solvents such as dimethyl sulfoxide, N, N-dimethylformamide, and hydrochloric acid were obtained from Himedia.

Synthesis of Polymer

The copolymer 2, 4-DBAF was synthesized from 2, 4-dihydroxybenzoic acid (0.1mol) and acrylamide (0.1mol) with formaldehyde (0.2mol) applying polycondensation technique, in 2Molar hydrochloric acid. The mixture of reactants was heated at 122^0C under reflux conduction for 5 hours, resulting in formation of a yellow resin-like product. Preliminary purification was carried out by washing with diethyl ether followed by hot distilled water. Further purification of the polymer, it was dissolved in 8% (w/v) sodium hydroxide solution and then precipitated by the incremental addition with (exclusive) mixture of concentrated chlorohydrin acid and distilled water. Resulting product existed finely ground and sieved. The polymer demonstrated excellent dissolvability within solvents such as DMSO, DMF, and THF, highlighting its strong compatibility with these organic media. However, it showed only partial solubility when tested in mineral acids, suggesting limited interaction under acidic conditions.

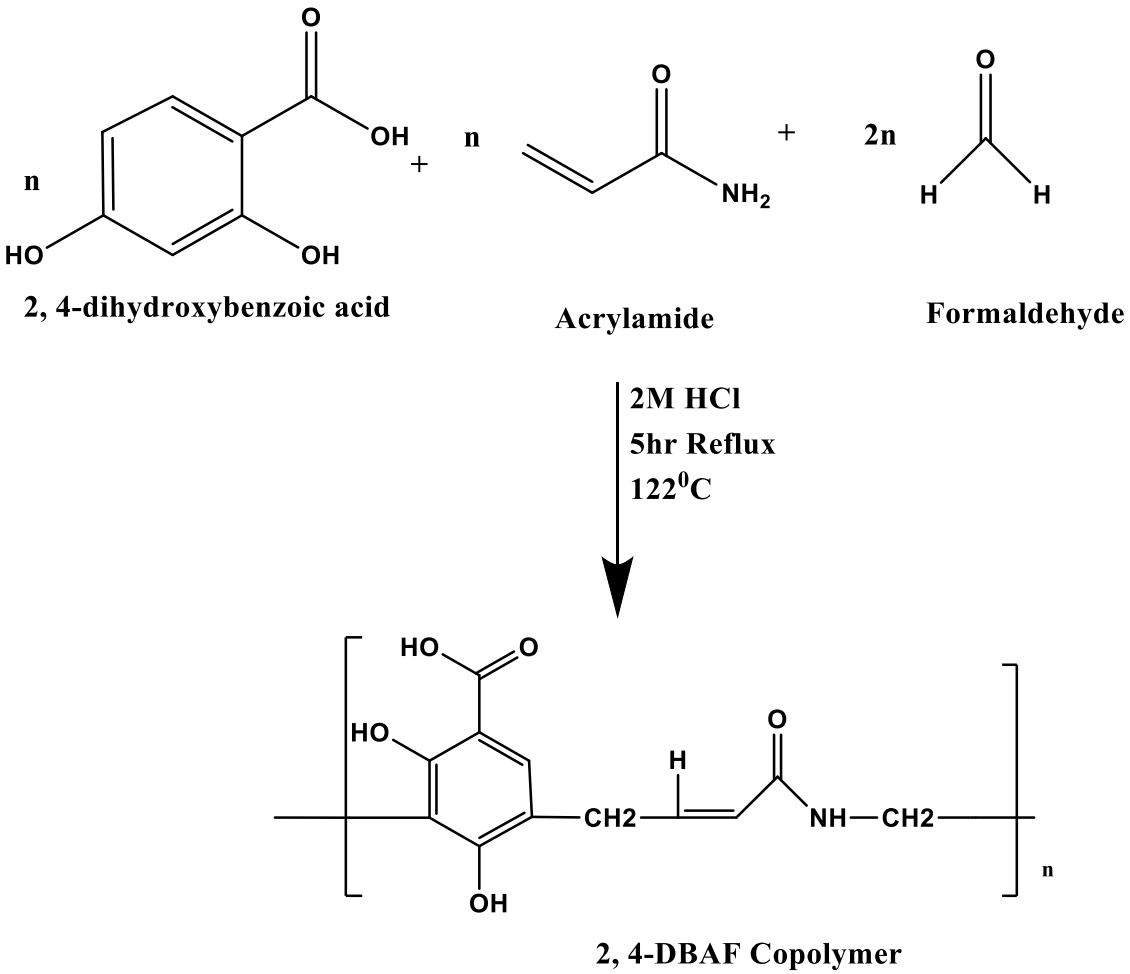

Figure 1: Synthesis of 2, 4-DBAF polymer

Instruments

The synthesized polymer resin was subjected to comprehensive physicochemical and structural characterization using a variety of analytical approaches. Elemental composition existed accomplish using a Perkin Elmer 789N QP-2010 recorder. Molecular weight exist regulate by Gel Permeation Chromatography, utilizing tetrahydrofuran in the role of eluent at a duration of 1 mL/min, with regulated employ polystyrene calibre. UV–Visible spectral studies were eminent in DMSO over a frequency spectrum of 200–800 nm. FTIR signal do measured using KBr pellets in the 4000–500 cm^{-1} scale. The ^{1}H NMR signals were obtained in DMSO-d_6 on a 400 MHz Bruker spectrometer. The polymer's exterior texture exist analysed using Scanning Electron Microscopy (SEM), while its crystalline properties were examine through X-ray Diffraction (XRD) analysis. Additionally, thermal stability along with decay study were evaluated using a Perkin Elmer TGA/DTA thermal analyser.

Physico-chemical characteristics

Physico-chemical characteristics of the polymer resin such as void volume fraction, solid content, true density, moisture content, and sodium exchange capacity were systematically examine using

established literature methods. These assessments offered important insights into the resin's structural features and ion-exchange capabilities

Percentage of moisture content

To regulate moisture present, 0.30 g of polymer was soaked in 35 mL of distilled water for 46 hours to allow swelling. The swollen resin was filtered, and surface moisture was gently detach with filter paper. It was then shriveled and weighed. Afterward, the polymer was desiccated in a drying oven at 90–98 °C for 8 hours, cooled and reevaluated. The moisture content (%) was evaluated from the dissimilarity between the swollen and dry weights of the resin.

The solid content (%)

$$\text{Solid content (\%)} = (W_d/W_b) \times 100 \text{---------- (1)}$$

Where:

Wd = Dried material (g)

Wb = Material before drying (g)

Moisture Content Calculation

The moisture content in percentage was examine using this equation

$$\text{Moisture content percentage} = 100 - \text{Solid (\%)} \text{ ---------- (2)}$$

True density

$$\text{True density} = \frac{Wp-W}{(Ww-Wpw)+(Wp-Ww)} \text{ ---------- (3)}$$

Where:

W = mass of empty bottle

Wp = mass of bottle with sample

Ww = mass of bottle with water

Wpw = mass of bottle with polymer and water

Volumetric Density

$$\text{Volumetric density} = \frac{Weight\ of\ sample}{Volume\ of\ sample} \text{ ---------- (4)}$$

To examine the fundamental physical characteristics of the composite material, the procedure described above was systematically applied. This allowed for the determination of key parameters, including solid content (%), moisture content (%), true density and apparent density. Each measurement was carried out using standard methods previously reported in the literature to ensure consistency and reproducibility.

Cation exchange capacity

The total ion-exchange capacity of the synthesized polymer represents the cumulative number of functional ion-exchange sites available per unit volume of the swollen polymer matrix. For this analysis, 2.0 g of dry polymer with a similar particle size of 30–60 mesh was accurately weighed and individually placed into 250 mL Erlenmeyer flasks. To each flask, 250 mL of a standardized 0.1 M

sodium hydroxide solution in 1 Molar sodium chloride was put on. The mixtures were endure to equilibrate for 24 hours with occasional shaking to ensure uniform interaction. After equilibration, 50 mL aliquots were withdrawn from each mixture and titrated with standardized 0.1 Molar hydrochloric acid. The complete cation exchanger was then examined based on the amount of sodium hydroxide consumed during the titration.

Ion-exchange analysis

Electrochemical analysis of metals at distinct electrolytes

The ion-exchange characteristics of the newly synthesized polymer were systematically studied through the batch equilibrium approach to determine its efficiency in selectively adsorbing metal ions such as Co^{2+}, Cd^{2+}, Pb^{2+}, and Hg^{2+}. This method was chosen for its simplicity and effectiveness in simulating ion-exchange conditions under controlled parameters. To begin, 25 mg of the polymer was accurately weighed and placed into separate, sterilize glass bottles. To each bottle, 25 mL of electrolyte solutions with varying normalities (0.1 N, 0.5 N, and 1.0 N) of NaCl, $NaClO_4$, and $NaNO_3$ were added. These electrolytes were used to evaluate the control of ionic concentration and the type of counter-ion on metal uptake behaviour. To maintain a consistent pH, an appropriate volume of 0.1 Molar hydrochloric acid or 0.1 Molar sodium hydroxide was added as needed. The mixtures were then vigorously stirred for 24 hours, allowing the polymer to swell fully and enhance its porosity and hydrophilic interaction, both of which are critical for efficient ion-exchange. Following the swelling period, 2 mL of 0.1 Molar metal salt solutions targeted metal ions were introduced into each bottle. After readjusting the pH to the desired value, the mixtures were stirred again for 24 hours to allow sufficient time for ion-exchange equilibrium to be established. After equilibration, the polymer was separated by purification method, and the resulting filtrate was collected. The quantity of unbound cation ions in the solution exist examine by titrating the filtrate with a standardized disodium salt solution of ethylenediaminetetraacetic acid (EDTA). This step enabled precise quantification of residual metal ion concentrations. In parallel, a blank experiment (without the polymer) was conducted under identical conditions to serve as a control and validate the accuracy of the results. The dissimilarity between the earliest and residual metal ion concentrations exist application to calculate the cation ion uptake capacity of the polymer using this equation:

$$Q = \frac{(Co - Ce)}{M} \text{ ---------- (5)}$$

Where:

Q = ion-exchange capacity

C_0 = initial concentration

C_e = final concentration

M = weight of the polymer

Analysis of metal ions at different pH

The impact of hydrogen ion concentration (pH) on the retention of metal ions was explored by systematically altering the pH values of the solution across a range from 1.5 to 6.0, utilizing a chosen electrolyte medium to stabilize the ionic strength. The modifications in pH were meticulously carried out using 0.1 M sulphuric acid (H_2SO_4) to lower the pH and 0.1 M sodium hydroxide (NaOH) to increase it. All experimental evaluations were executed at a stable temperature of 25 °C, ensuring uniform thermal conditions throughout the metal ion adsorption experiments

Analysis of rate of metal ion uptake

To establish the required equilibrium time for optimal metal ion adsorption under the specified experimental conditions, a series of time-based adsorption experiments were conducted. These trials were structured to evaluate the amount of metal ion retained by the polymer at different time intervals, employing a constant electrolyte medium namely, and 25 mL of 0.1 M sodium perchlorate ($NaClO_4$) solution

For every instance, the cumulative amount of metal ion bound at a specific time interval was quantified and expressed as a percentage relative to the total metal ion uptake at equilibrium. This methodology facilitated the assessment of adsorption kinetics, revealing the rate at which metal ions interact with the functional binding sites present on the polymer framework. The proportion of metal ion adsorption at any distinct time was calculated using the following formula:

$$\text{Metal ion uptake} = \frac{(initial\ concentration - final\ concentration)}{initial\ concentration} X\ 100 \text{ -------- (6)}$$

Thermal analysis

Thermogravimetric analysis (TGA) was employed to investigate the thermal decomposition attribute and evaluate the heat-stable of the synthesized polymer. The TGA measurements provided precise information regarding the degradation behaviour of the materials across a defined temperature range. Using the TG data, critical kinetic and thermodynamic parameters, such as activation energy and entropy changes, were calculated. These values were obtained using two widely accepted non-isothermal kinetic models: the (SW) method and (FC) method. Together, these approaches offered a thorough understanding of the polymer's thermal properties and its potential applicability in thermally demanding environments.

RESULTS & DISCUSSION

Elemental analysis of 2, 4-DBAF Polymer

Micro analytical techniques were utilized to examine the elemental makeup of the synthesized 2, 4-DBAF polymer, with particular emphasis on the amount of carbon (C), hydrogen (H), nitrogen (N), and sulphur (S). The analysis was conducted to verify the stoichiometry of the polymer and confirm its structural integrity. The investigational values acquire were obtain to be in very similar with the theoretical values calculated based on the proposed chemical structure. From the evidence found, the empirical formula of the polymer was established, and the actual molecular weight of a standalone repeating unit was examine accordingly. These values are systematically presented in Table 1. Which outlines the theoretical and experimental elemental percentages for each constituent element.

Table 1: Elemental Analysis of 2, 4-DBAF Polymer

Polymer	Percentage of Carbon Observed (Cal.)	Percentage of Hydrogen Observed (Cal.)	Percentage of Nitrogen Observed (Cal.)	Empirical Formula of repeated unit	Empirical Formula Weight
2, 4-DBAF	52.60 (53.83)	3.11 (4.18)	6.42 (8.37)	$C_{15}H_{14}N_2O_5$	334.35

Molecular Weight determination of 2, 4-DBAF Polymer

The molecular weight of the synthesized polymer was examine by using the conventional Gel Permeation Chromatography (GPC) technique. This method allows for the accurate estimation of the molecular weight distribution of polymers based on their size in solution. In this analysis, tetrahydrofuran (THF) was employed as the mobile phase, maintained at a constant discharge of 1 mL/min. A set of polystyrene standards with known molecular weights was used for calibration, allowing for the generation of a standard curve against which the molecular weight of the polymer sample was compared. The results obtained, including the number-average molecular weight (Mn) is summarized in Table 2, providing insights into the molecular characteristics of the prepared polymer.

Table 2: Molecular Weight determination of 2, 4-DBAF Polymer

Polymer	Empirical weight (gm)	Number average molecular weight ($\bar{}_{Mn}$)
2, 4-DBAF	312	3235

Spectral studies

UV-Visible Spectra of 2, 4-DBAF Polymer

The UV–visible absorption spectra of the synthesized 2,4-DBAF polymer were recorded using dimethyl sulfoxide (DMSO) as the solvent, over a wavelength range of 200–800 nm. The spectral data, as depicted in Figure 2, reveal two distinct absorption maxima located at 266.50 nm and 305.50 nm. The absorption band at 266.50 nm, exhibiting higher intensity, is assigned to a $\pi \rightarrow \pi^*$ electronic transition. This transition is commonly associated with the aromatic nucleus, confirming the conjugated π-electron system in the copolymer structure. The second band at 305.50 nm, with lower intensity, is attributed to an $n \rightarrow \pi^*$ transition, likely originating from the presence of non-bonding electron pairs on functional groups such as –NH. The presence of hydroxyl groups in the polymer structure is supported by a hyperchromic shift (an increase in absorbance, i.e., higher ε_{max} values), which is typical in systems where electron-donating groups enhance π-electron density. This behavior is consistent with well-documented observations in benzene derivatives, where $\pi \rightarrow \pi^*$ transitions dominate in aromatic rings, and $n \rightarrow \pi^*$ transitions are often linked to lone pairs present on heteroatoms like nitrogen or oxygen.

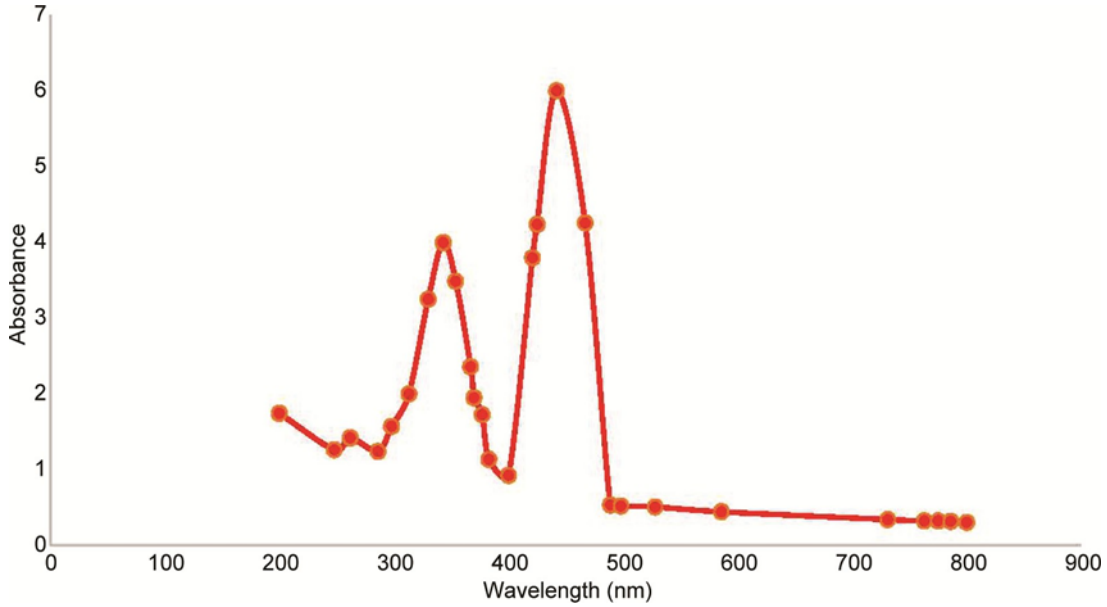

Figure 2: Ultraviolet-Visible spectrum of 2, 4-DBAF Polymer

FTIR spectra of 2, 4-DBAF Polymer

The FTIR spectrum of the synthesized 2,4-DBAF copolymer is illustrated in Figure 3, with corresponding absorption band assignments summarized in Table 3. The spectrum provides valuable insights into the functional groups present in the polymer backbone and confirms key structural features. A broad absorption band centered at approximately 3325 cm^{-1} is observed, which is characteristic of the O–H stretching vibration associated with phenolic hydroxyl groups. The broadness of this peak suggests the presence of intermolecular hydrogen bonding, a common feature in phenolic systems. A sharp and intense band at 1625 cm^{-1} is attributed to the C=O stretching vibration of an aromatic carbonyl group (Ph–CO), indicating the successful incorporation of carbonyl functionalities into the polymer matrix.

Medium-intensity peaks at 2978 cm^{-1} and 2600 cm^{-1} correspond to C–H stretching vibrations of methyl (–CH_3) and methylene (–CH_2) groups, respectively, suggesting aliphatic character in segments of the polymer chain. Another medium band observed at 2939 cm^{-1} is associated with –NH– stretching, which may originate from the pyridine moiety present in the polymer. A weak band appearing at 1482 cm^{-1} is indicative of aromatic C=C stretching, confirming the existence of conjugated aromatic rings in the polymer backbone. Moreover, a sharp and strong peak at 1373 cm^{-1} is assigned to the methylene bridge (–CH_2–) group, suggesting the presence of such linkages within the polymer structure, which likely result from condensation reactions during polymer formation. These spectral features collectively support the structural composition of the 2, 4-DBAF polymer and validate the proposed molecular framework.

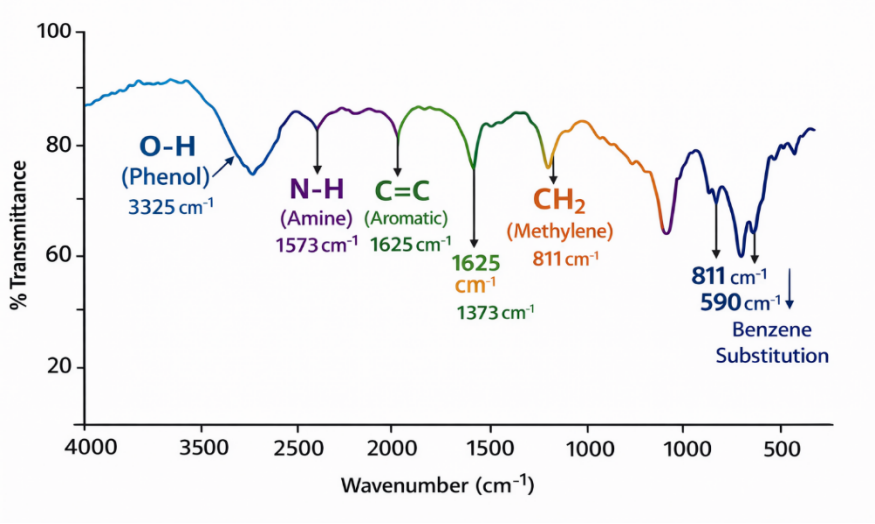

Figure 3: FTIR spectra of 2, 4-DBAF Polymer

Table 3: FT- IR spectral data of 8-HQ-5-SAAF Polymer

Assignment	Expected wave number (cm^{-1})	Observed wave number (cm^{-1})
Ph-OH	3100-3500	3325(broad, strong)
>NH (amino)	1560	1573(sharp, strong)
Phenyl ring	1445-1485	1625(sharp, medium)
$>CH_2$ (methylene bridges)	1250-1360	1373(weak, medium)
1,2,3,4,5 substitution in benzene skeleton	557.9-900	590.86 and 811.52 (broad ,strong)

Proton ^{1}H NMR spectra of 2, 4-DBAF Polymer

The ^{1}H NMR spectrum of the 2,4-DBAF polymer is displayed in Figure 4, with corresponding spectral assignments presented in Table 4 and supported by literature [31, 37, 38]. The spectral dada provides key statistics regarding the proton environments in the polymer chain, confirming the expected structural features. A medium-intensity singlet observed in the δ 2.5–3.0 ppm range corresponds to the methyl protons of the Ph–CO–CH_2 group. The amino proton linked to the –C–NH–CS– moiety appears as a triplet between δ 3.0 and 4.1 ppm, aligning with literature findings [37]. A strong signal in the δ 3.5–4.5 ppm range is attributed to the methylene (–CH_2–) protons within the polymer backbone. Aromatic protons give rise to a weak, unresolved pattern between δ 6.5 and 8.5 ppm, characteristic of substituted benzene rings. Additionally, a weak signal between δ 7.5 and 8.2 ppm is assigned to the phenolic –OH proton, confirming the presence of phenolic groups in the polymer structure [38].

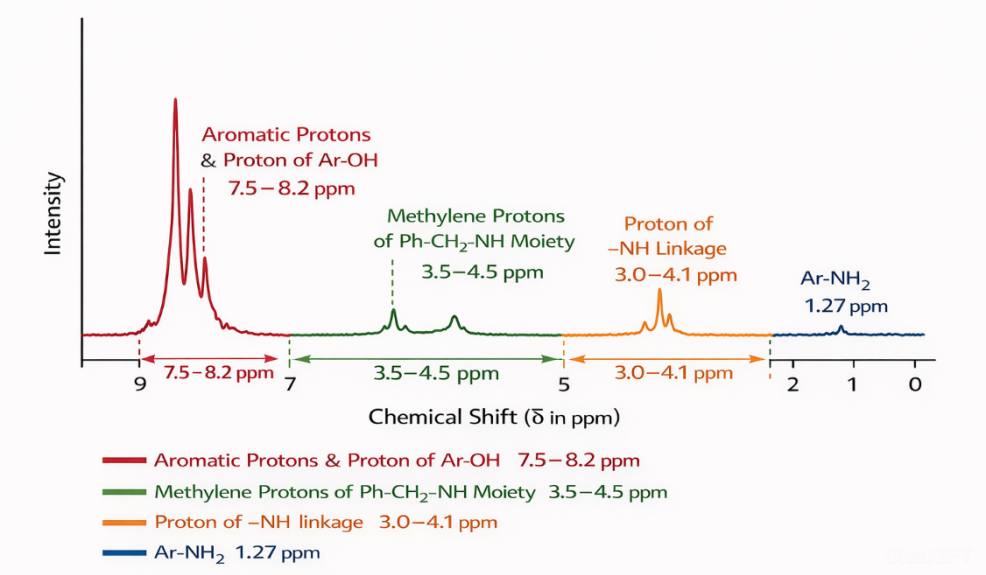

Figure 4: ^{1}H NMR Spectra of 2, 4-DBAF Polymer

Table 4: ^{1}H NMR Spectral data of 8-HQ-5-SAAF Polymer

Proton assigned	**Chemical shift (δ) ppm of 2, 4-DBAF polymer**
Aromatic proton (unsymm- pattern)	7.5-8.2
Proton of –NH linkage	3.0-4.1
Methylene proton of Ph-CH_2-NH moiety	3.5-4.5
Proton of Ar-OH	7.5-8.2
Ar-NH_2	1.27

Scanning electron microscopy of 2, 4-DBAF Polymer

The surface topography of the synthesized 8-HQ-5-SAAF polymer was inspect using scanning electron microscopy (SEM), as presented in Figure 6. The micrograph reveals the formation of spherical structures (spherules) with a smooth, polycrystalline surface texture, which is indicative of semi-crystalline behaviour in the polymer matrix. Additionally, the presence of a fringed surface pattern suggests a composite structure containing both amorphous and crystalline regions. The observed degree of crystallinity appears to correlate with the acidity of the monomer units, implying that monomer composition influences the overall microstructure. The amorphous features are characterized by a densely packed surface, interspersed with deep pits, which are potential active sites for interaction in ion-exchange processes. The yellow coloration of the polymer and the fringed morphology observed across the surface further illustrate the transition zone between amorphous and crystalline domains. Moreover, the SEM image reveals the presence of small holes and surface cracks, likely resulting from trapped air voids during the polymerization or drying process. These imperfections could serve as advantageous structural features, enhancing the polymer's surface area and making it potentially more effective in adsorption or ion-exchange applications.

The crystal-like formations visible in the copolymer solution suggest a larger-scale molecular

organization, resembling spherulitic structures often observed in semi-crystalline polymers. These spherulites, typically spanning a few millimeters in diameter, reflect the polymer's self-organizing capacity during solidification.

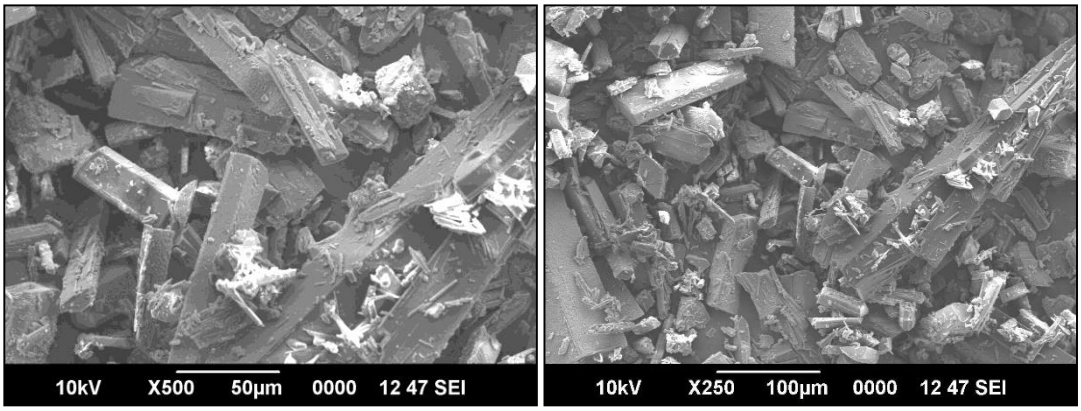

Figure 5: SEM images of 2, 4-DBAF Polymer

Ion-exchange studies

The ion-exchange capacity of the prepared polymer resins was evaluated using the batch equilibrium technique developed by Gregor and Degeiso et al. This method is widely accepted for assessing the sum of active ion-exchange places available in polymeric materials under equilibrium conditions.

Procedure

To investigate the ion-exchange performance, the finely powdered form of the synthesized polymer was utilize for the uptake of choose divalent metal ions, namely Co^{2+}, Zn^{2+}, Cu^{2+}, Ni^{2+}, and Pb^{2+}. The experiments were carried out using the nitrate salts of these metals in aqueous solution, deliberately avoiding their chloride or sulfate counterparts to prevent unwanted precipitation of the target metal ions. This approach allowed for a controlled assessment of the polymer's chelation-based ion-exchange properties. The study focused on evaluating the polymer's efficiency in cation exchange under varied experimental conditions, providing insights into its selectivity, affinity, and practical applicability in removing heavy metals from solution.

.

Preparation of standard solutions

a) **Electrolyte Solutions**: Stock solutions (1.0 M) of various electrolytes—including sodium chloride (NaCl), sodium nitrate ($NaNO_3$), sodium sulfate (Na_2SO_4), and sodium perchlorate ($NaClO_4$)—were prepared in double distilled water. From these stock solutions, working concentrations of 0.01 M, 0.1 M, and 0.5 M were subsequently prepared by appropriate dilution.

b) **Metal Nitrate Solutions**: Stock solutions (0.1 M) of selected hydrated metal nitrate salts including ferric nitrate nonahydrate [$Fe(NO_3)_3 \cdot 9H_2O$], cobalt nitrate hexahydrate [$Co(NO_3)_2 \cdot 6H_2O$], nickel nitrate hexahydrate [$Ni(NO_3)_2 \cdot 6H_2O$], copper nitrate trihydrate [$Cu(NO_3)_2 \cdot 3H_2O$], zinc nitrate hexahydrate [$Zn(NO_3)_2 \cdot 6H_2O$], and lead nitrate [$Pb(NO_3)_2$]were prepared using double-distilled water to maintain solution uniformity and minimize contamination.

c) **EDTA Solution**: A 0.1 M solution of the disodium salt of ethylenediaminetetraacetic acid (EDTA) was prepared and employed as the standard titrant in complexometric titrations for determining unbound metal ions.

Investigation of Metal Ion Binding Efficiency in the Presence of Diverse Electrolytes at Different Concentration Ranges

The impact of dissimilar electrolyte anions namely perchlorate (ClO_4^-), chloride (Cl^-), nitrate (NO_3^-), and sulfate (SO_4^{2-}) on the equilibrium between metal ions and the polymer was thoroughly examined over a range of concentrations. It was noted that the nature and concentration of the electrolyte present in the solution had a considerable impact on the extent of metal ion adsorption by a constant amount of resin, as illustrated in Table 5. In systems incorporating perchlorate (ClO_4^-) and chloride (Cl^-) ions, the adsorption performance for Ni^{2+} and Cu^{2+} ions showed enhancement with increasing electrolyte concentration. Conversely, the adsorption capacities for Zn^{2+}, Co^{2+}, and Pb^{2+} ions declined with increasing levels of these same electrolytes [35–36]. A comparable trend was also noted in the presence of nitrate ions, where higher concentrations of $NaNO_3$ promoted the adsorption of Ni^{2+} and Cu^{2+}, while diminishing the uptake of Zn^{2+}, Co^{2+}, and Pb^2

Conversely, in the presence of sulfate ions (SO_4^{2-}), the adsorption of all investigated metal ions (Ni^{2+}, Cu^{2+}, Co^{2+}, Zn^{2+}, and Pb^{2+}) decreased consistently as the concentration of Na_2SO_4 increased. This behavior is attributed to the differing complexation tendencies of the electrolytes: ClO_4^-, Cl^-, and NO_3^- form relatively weak complexes with Ni^{2+} and Cu^{2+}, thereby enhancing their availability for ion exchange. In contrast, SO_4^{2-} forms strong complexes with Ni^{2+} and Cu^{2+}, thereby suppressing their adsorption.

Table: 5. Assessment of Various Electrolyte Impacts on the Adsorption of Multiple Metal Ions by the 2, 4-DBAF Polymer.

Metal ion	Electrolyte (mol./l)	pH	Amount of metal ion adsorbed (mg per gram of resin) in the presence of			
			$NaClO_4$	NaCl	$NaNO_3$	Na2SO4
Fe^{2+}	0.01	2.5	0.41	0.29	0.19	0.88
	0.05		0.47	0.36	0.32	0.64
	0.10		0.58	0.48	0.44	0.52
	0.50		0.80	0.76	0.64	0.43
	1.00		0.84	0.82	0.72	0.38
Cu^{2+}	0.01	4.5	0.1	0.08	0.06	0.64
	0.05		0.2	0.13	0.09	0.58
	0.10		0.34	0.25	0.14	0.48
	0.50		0.46	0.32	0.28	0.32
	1.00		0.56	0.46	0.42	0.18

Cd^{2+}	0.01	5.0	0.33	0.11	0.12	1.14
	0.05		0.45	0.23	0.24	1.11
	0.10		0.67	0.34	0.34	0.78
	0.50		0.93	0.78	0.56	0.68
	1.00		0.98	1.22	0.65	0.34
Zn^{2+}	0.01	5.0	0.22	0.09	0.09	0.70
	0.05		0.37	0.14	0.14	0.62
	0.10		0.44	0.24	0.26	0.47
	0.50		0.58	0.56	0.46	0.38
	1.00		0.77	0.72	0.58	0.19
Ni^{2+}	0.01	4.5	0.12	0.01	0.09	0.53
	0.05		0.20 0.28	0.04	0.11	0.45
	0.10		0.34	0.7	0.17	0.32
	0.50		0.44	0.25	0.20	0.26
	1.00		0.48	0.29	0.26	0.11
Pb^{2+}	0.01	6.0	0.52	0.23	0.23	1.62
	0.05		0.58	0.46	0.42	1.22
	0.10		1.45	0.76	0.78	0.89
	0.50		2.66	1.67	1.66	0.61
	1.00		2.88	2.17	1.92	0.42

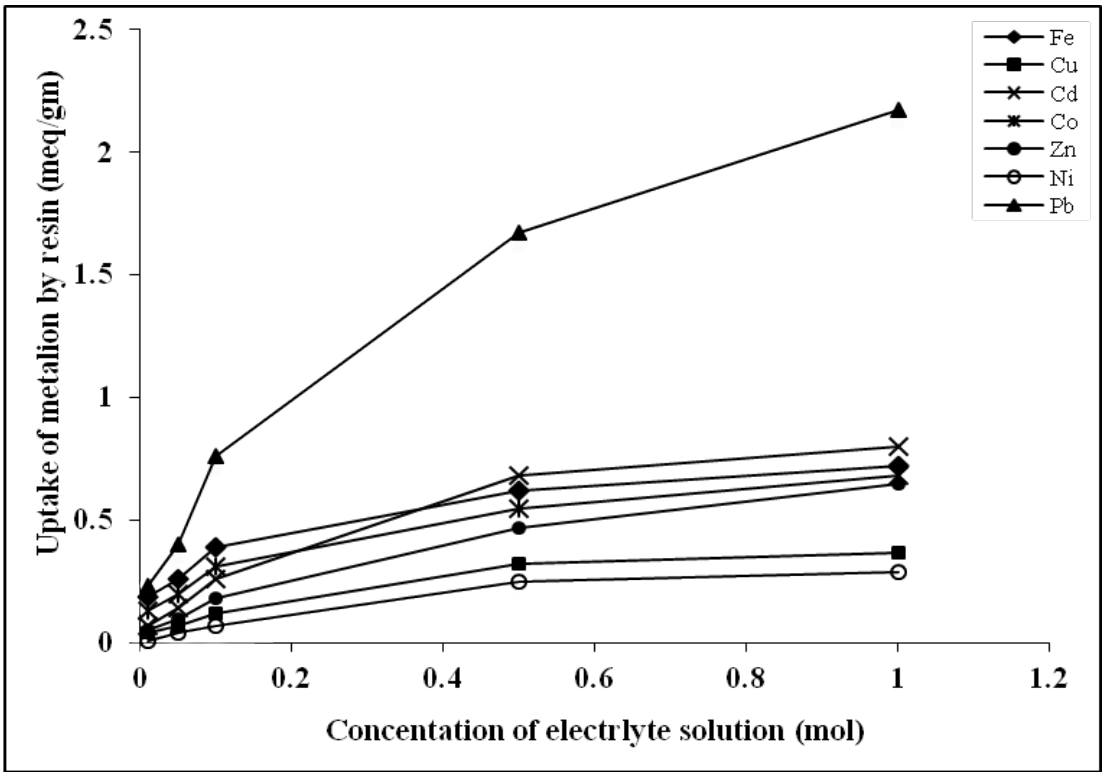

Fig. 6. Rate of metal ion uptake 2, 4-DBAF Polymer

Investigation of Metal Ion Uptake across Different pH Conditions

The variation in metal ion distribution between the aqueous medium and the 2,4-DBAF polymer phase as a function of pH is outlined in Table 6. The distribution ratio (D), representing the efficiency of metal ion binding by the polymer, exhibited a noticeable increase with the elevation of solution pH [37–38]. To avoid metal ion precipitation or instability under alkaline conditions, the pH range for each metal ion was carefully restricted to its appropriate operational limits during experimentation although the uptake increases with pH for all tested cations, the degree of enhancement varies among the unalike metal ions. Notably, the allocation ratios for Cu (II) and Ni (II) were significantly higher than those of the other metal ions, indicating a stronger affinity of the polymer for these cations. In the company of studied metal ions, the order of distribution was found to follow the sequence: cupper > nickel > cobalt> zinc > lead.

The trend suggests that Cu (II) and Ni (II) exhibit additional complex interaction behaviour with the polymer matrix, likely due to favorable coordination or chelation effects. The findings provide important insights for optimizing pH conditions during selective metal ion separation from mixed-metal solutions.

Table: 6. Distribution Coefficient of Different Metal Ions as Influenced by pH Using 2, 4-DBAF Polymer.

Metal ion	**Effect of pH Variation on the Distribution Coefficient of Metal Ions**									
	1.5	**1.75**	**2.0**	**2.5**	**3.0**	**3.5**	**4.0**	**5.0**	**6.0**	**6.5**
Fe3+	112.4	128.9	146.9	387.6	-	-	-	-	-	-

Cu2+	-	-	-	42.09	56.79	61.77	72.72	96.29	146.33	192.62-
Cd2+	-	-	-	56.92	64.50	167.08	207.41	168.76	254.34	284.36
Zn2+	-	-	-	76.7	124.83	188.55	268.67	466.67	419.05	544.14
Ni2+	-	-	-	38.30	44.009	68.136	92.52	72.72	114.64	326.34
Pb2+	-	-	-	72.36	84.05	144.59	378.95	684.06	1428.3	2466.1

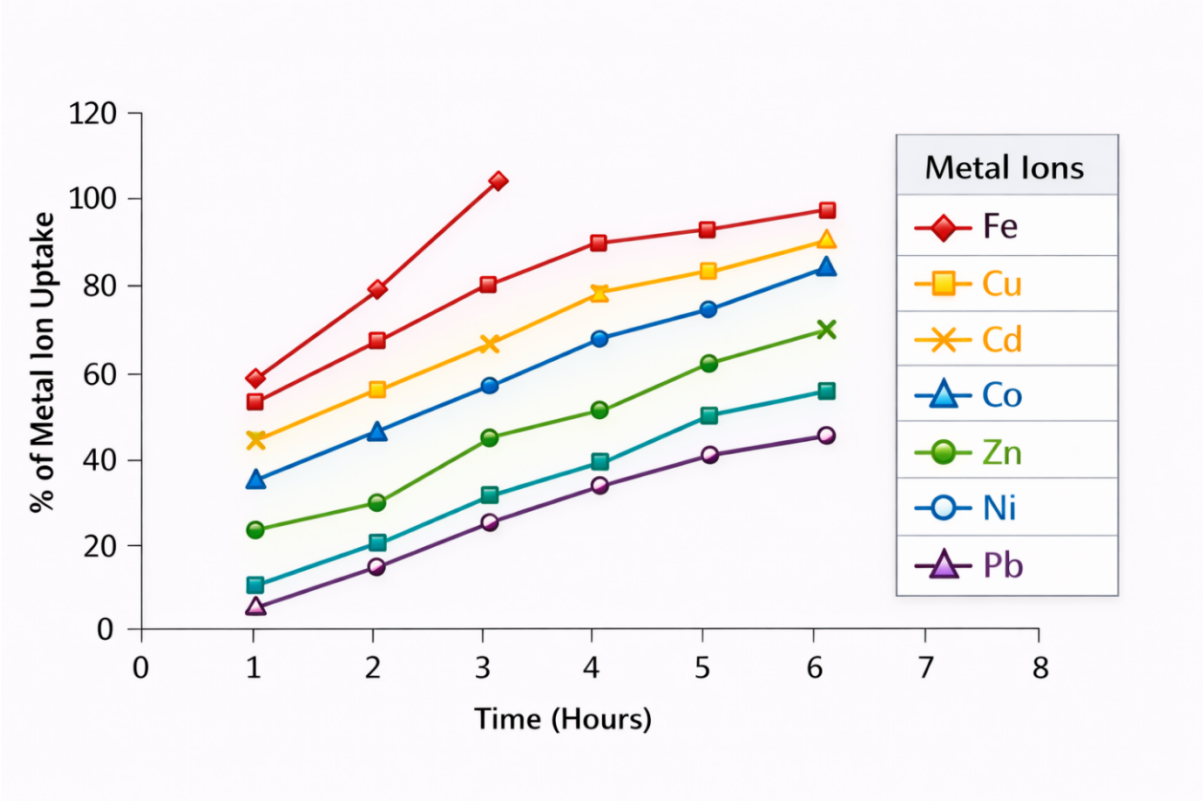

Fig. 7. Effect of Ph on cation exchange capacity

Kinetic Evaluation of Metal Ion Uptake over Time

The adsorption kinetics of metal ions by the prepared polymer were assessed by identifying the duration required to establish equilibrium between the polymer matrix and the metal ions under standardized laboratory conditions. A series of batch-mode adsorption experiments were carried out, during which the cumulative amount of metal ions taken up by the polymer was recorded at multiple time points (1, 2, 3, … up to 24 hours) at room temperature. For each experimental run, 25 mg of the polymer sample was combined with 25 mL of 1 M sodium nitrate ($NaNO_3$) solution, and the pH was finely adjusted to the target value using 0.1 M hydrochloric acid (HCl) or 0.1 M sodium hydroxide (NaOH). It was presumed that equilibrium was attained within a 24-hour period under these specified

conditions. After each predetermined contact time, the suspension was filtered, the polymer was thoroughly washed with distilled water, and the resulting filtrate was collected. The residual concentration of non-adsorbed metal ions in the filtrate was then determined via complexometric titration using 0.1 M EDTA along with a suitable metallochromic indicator [39–42].

The amount of metal ions adsorbed at each time point was calculated by evaluating the difference between the initial concentration and the residual concentration of metal ions present in the filtrate. The rate of adsorption was expressed as the percentage of metal ions adsorbed at a specific time relative to the total amount adsorbed at equilibrium. The percentage of metal ion uptake over a defined time period was determined using the formula given below

$$\text{Metal Ion uptake (\%)} = \left(\frac{X}{Y}\right) X100 \text{ ----- (7)}$$

Where:

X = metal ion adsorbed at time t (e.g., after 1 hour)

Y = metal ion adsorbed at equilibrium (after 24 hours)

This kinetic analysis provides insights into the adsorption rate and efficiency of the polymer, which are critical for practical applications in metal ion removal from aqueous systems.

Table: 6. Assessment of Differences in Metal Ion Binding Rates by 2, 4-DBAF Polymer.

Metal ion	Variation in Metal Ion Adsorption Efficiency with Contact Time (hrs)					
	1	**2**	**3**	**4**	**5**	**6**
Fe3+	62.6	85.2	105.6	-	-	-
Cu2+	15	25	38	45	55	62.7
Cd2+	19.2	28	46	52	58.2	68.5
Zn2+	38	46	56	65	68.5	88.5
Ni2+	6	14	28	34.4	48	52.4
Pb2+	42	54	68	78	88	90

Determination of the Ion-Exchange Potential

The ion-exchange capacity of the newly synthesized polymer resin was evaluated using the procedure described below. A 25 mg portion of the resin was dispersed in 50 mL of double-distilled water, followed by the addition of 25 mL of 0.5 M sodium acetate solution. The mixture was stirred gently for 2 to 5 minutes to facilitate the exchange of H^+ ions from the resin with Na^+ ions from the sodium acetate. This ion exchange resulted in the formation of acetic acid, which remained in the aqueous phase, while sodium ions were adsorbed onto the resin. Following the exchange process, the suspension was filtered, and the collected filtrate was titrated with 0.5 M sodium hydroxide to determine the concentration of released hydrogen ions. The ion-exchange capacity (IEC) of the polymer resin was then calculated using the following relation:

$$\text{Ion-exchange capacity (mmol/g)} = \frac{X \times Y}{Z} \text{ ---------- (8)}$$

Where:

X = Molarity (mol/L)
Y = Volume (mL)
Z = Weight of the sample (mg)
The determined cation-exchange capacity of the synthesized polymer was further compared with that of commercially available ion-exchange resins to evaluate its relative efficiency. The adsorption of metal ions by the polymer was examined under batch-mode conditions at ambient temperature, with a contact duration of 24 hours—deemed sufficient to achieve equilibrium. The experimental setup included the following conditions:
Metal Nitrate Concentration: 0.1 $mol \cdot L^{-1}$
Volume of Metal Ion Solution: 2 mL
Volume of Electrolyte Solution: 25 mL
Mass of Polymer Resin Used: 25 mg
To evaluate the metal ion uptake parameter (D), the subsequent mathematical expression was applied

$$D = \frac{Mass\ of\ Metal\ Ion\ Retained\ by\ 1\ g\ of\ Polyme}{concentraction\ of\ metal\ ion\ per\ millimeter\ of\ solution} \text{ ---------- (9)}$$

Metal ion retention efficiency (%) was determined using the equation given below

$$\text{Adsorption Efficiency of Metal Ions (\%)} = \left(\frac{Mass\ of\ Metal\ Ion\ Retained\ by\ the\ Adsorbent}{Quantity\ of\ Metal\ Ions\ Adsorbed\ at\ Equilibrium}\right) X100 \text{ ---- (10)}$$

These values provide a quantitative measure of the adsorptive capacity and efficiency of the polymer resin in removing metal ions from aqueous systems.

Thermogravimetric analysis of 2, 4-DBAF Polymer

The thermal performance of the 2, 4-DBAF polymer was discover through thermogravimetric analysis (TGA), with the thermo gram presented in Figure 8.A and Figure 8.B The an assessment was performed across temperature variation of 40°C to 700°C, and the thermal decomposition pattern exhibited three distinct stages [42]. In the first stage (40°C–120°C), observed a reduction in a minor weight, corresponding to the liberation of physically entrapped water molecules from within the crystalline regions of the polymer matrix. This phase accounted for a mass loss of 5.64% (observed), closely matching the calculated value of 5.69%. The second phase of decomposition occurred between 120°C & 380°C, marked by a gradual and significant mass reduction. This phase involved the breakdown and elimination of various functional groups, including –OH, and $–CH_2–NH–C=NH–CH_2–$ moieties. The total mass loss during this stage was 56.27% (experimental) and 56.35% (theoretical), indicating good agreement between observed and calculated values. A third decomposition phase was evident from 290°C to 460°C, contributing to a further weight loss of 71.85% (observed) compared to 70.33% (calculated). This phase reflects the degradation of more thermally stable units within the polymer backbone. The final degradation stage began around 520°C and sustained up to 700°C, assign to the complete breakdown away the polymer framework and elimination of the remaining polymeric residue. These results highlight the multi-stage thermal degradation pattern of the 2, 4-DBAF polymer, confirming its complex decomposition mechanism and providing valuable insights into its thermal stability and structural integrity under elevated temperatures.

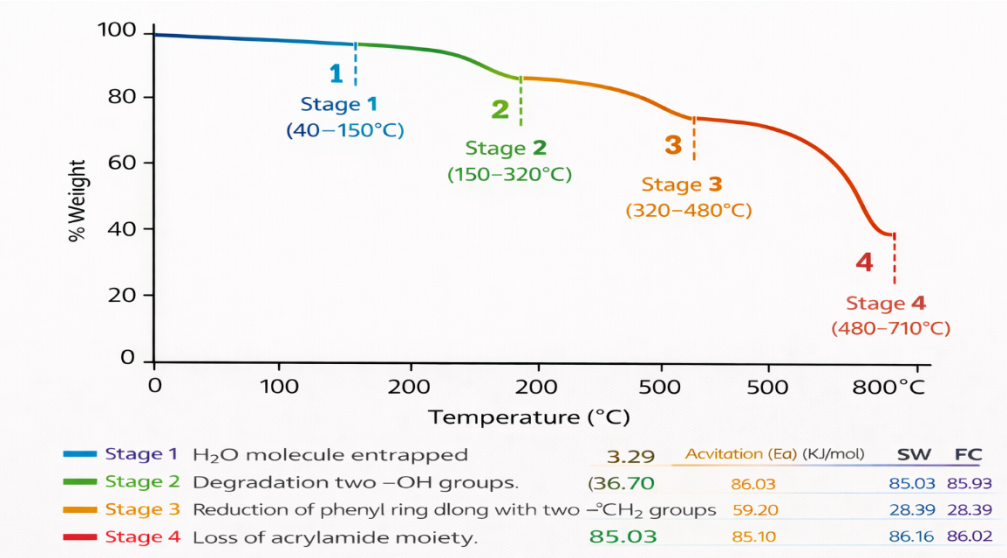

Figure 8.A. Thermogravimetric curve of 2, 4-DBAF Polymer

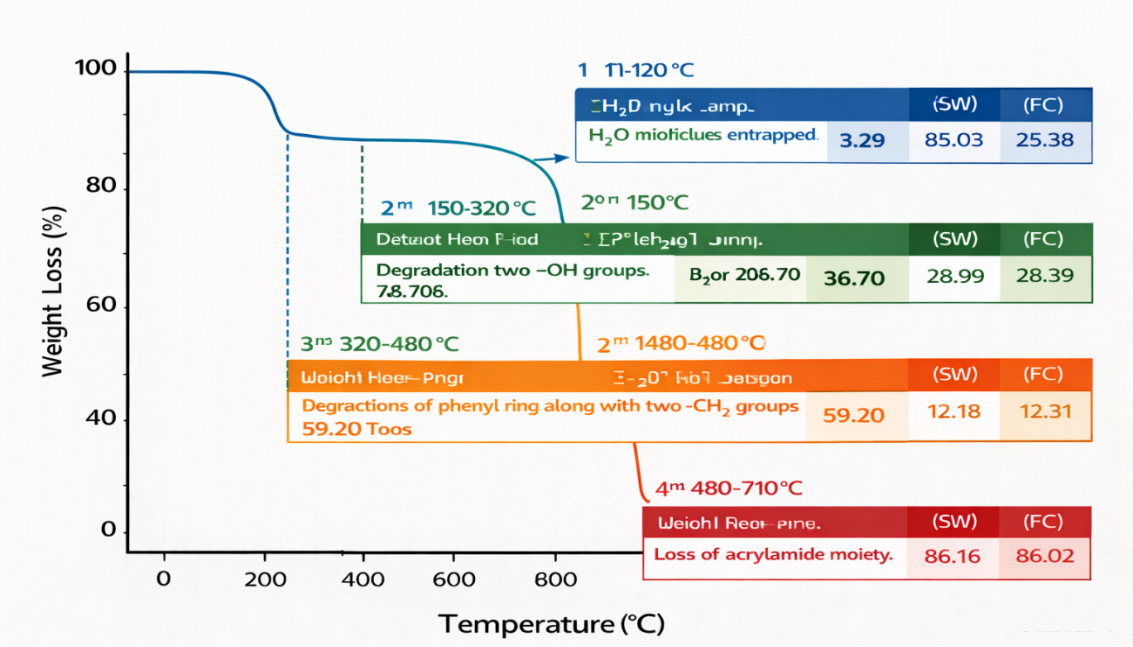

Figure 8.B. Thermogravimetric curve of 2, 4-DBAF Polymer

Sharp-Wentworth Method

The (SW) method were employed to regulate the activation energy (Ea) of the thermal degradation process. The following expression was used for the calculation:

$$\text{Log}\left[\frac{dc/dt}{1-c}\right] = log\ log\left(\frac{A}{\beta}\right)\frac{-Ea}{2.303\,R}\cdot\frac{1}{T} \text{ ------- (11)}$$

Where:

$\frac{dc}{dt}$ = Change in Weight Loss Fraction as a Function of Temperature

C = Degradation extent at time t

B = Linear heating rate

R = Universal gas constant

T = temperature (in Kelvin)

A = Frequency factor

Ea = Activation energy (kJ/mol)

A plot of

$$\text{Log } \frac{\left(\frac{dc}{dt}\right)}{1-c} / \frac{1}{T} \text{ ------- (12)}$$

Generate a straight line to evaluated the activation energy from the slope

$$\text{Slope} = \frac{-Ea}{2.303R} \text{ -------- (13)}$$

This graphical method, as illustrated in Figure 9, provides a reliable estimate of the activation energy for thermal decomposition, allowing further insight into the kinetic parameters of the polymer resin.

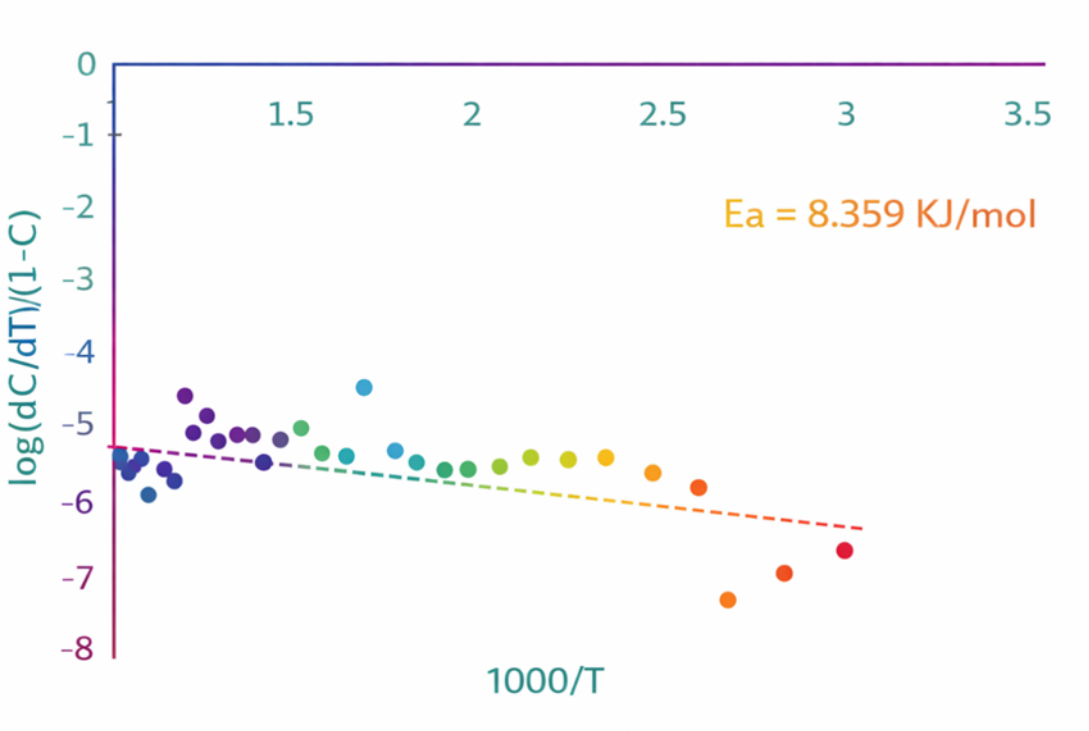

Figure 9. (SW) Activation energy graph of 2, 4-DBAF Polymer

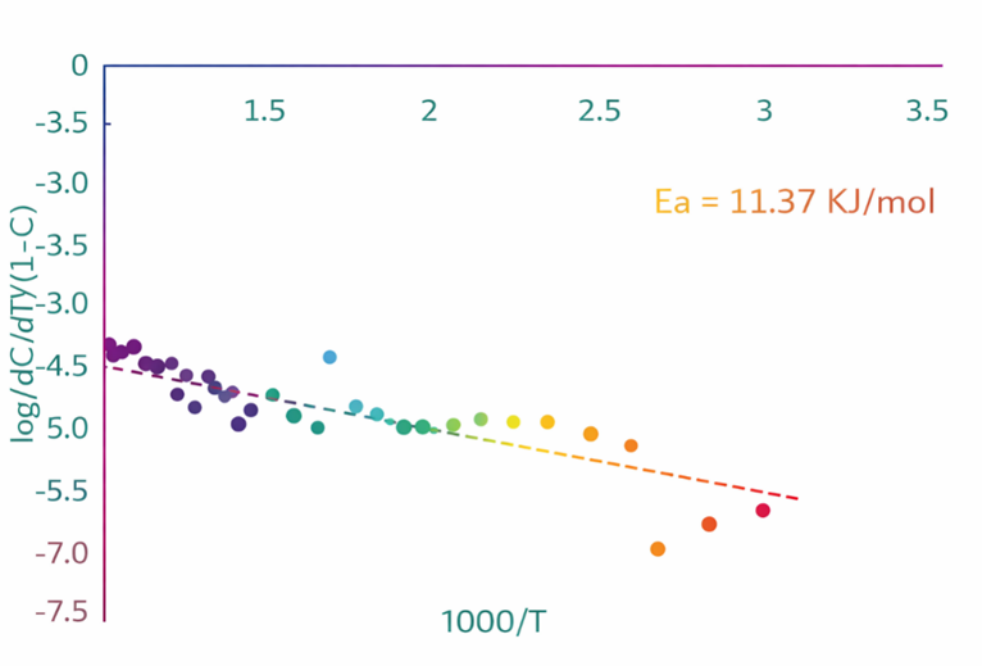

Figure 10. Sharp-Wentworth graph of 2, 4-DBAF Polymer

Freemann-Carroll method

The Freeman–Carroll method was also employed to judge the activation energy (Ea) and the reaction rate (n) of the thermal decay of the polymer resin. The equation used for this purpose is as follows:

$$\frac{\Delta log\,(\frac{dw}{dt})}{\Delta log log\,Wr} = \frac{Ea}{2.303R} \cdot \frac{\Delta(\frac{1}{T})}{\Delta Log\,Wr} + n \text{ ---------- (14)}$$

Where:

$\frac{dw}{dt}$ = Mass Accumulation Rate as a Function of Time

$W_r = W_C - W$

Wc= Decreased Mass Observed Upon Completion of the Reaction

W = Decrease in Sample Mass at a Given Time t

Ea= Activation energy (kJ/mol)

R = Universal gas constant

T = Absolute temperature (K)

n = Reaction rate

By analysing the thermogravimetric findings of the polymer and adopting a strategy of both (FC) **(**Figure 11) and (SW) (Figure 10) methods, the activation energy was evaluated. The results obtained by both techniques were found to be in close agreement, confirming the reliability of the kinetic parameters derived from the thermal breakdown behaviour for the polymer resin.

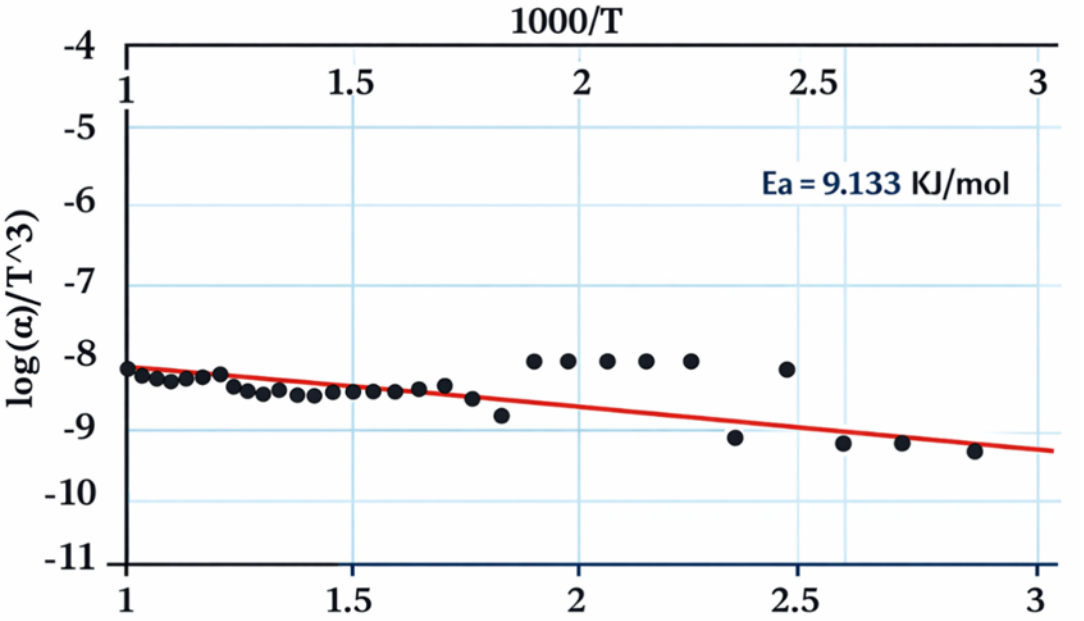

Figure 11. Freeman-Carroll Activation energy graph of 2, 4-DBAF Polymer

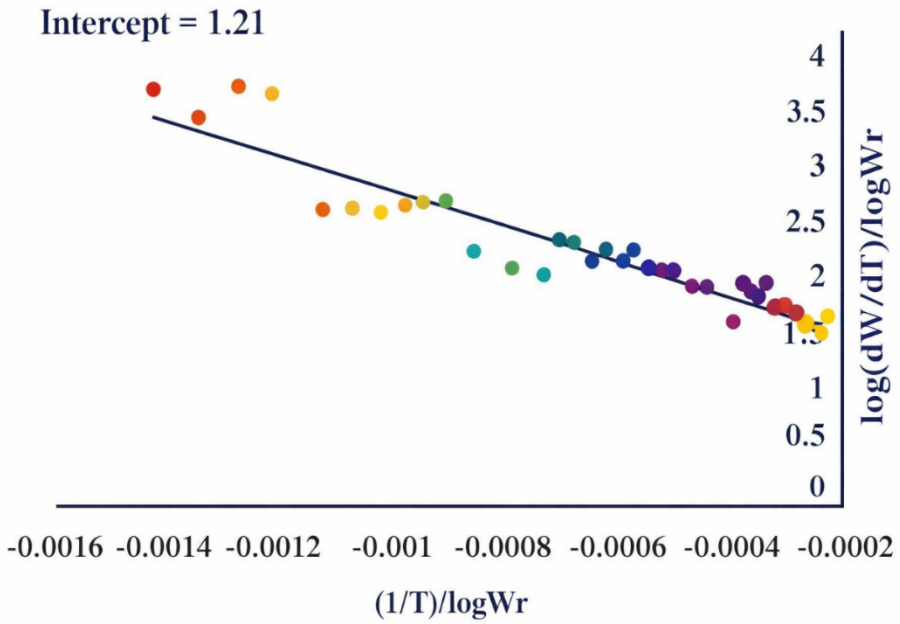

Figure 12. (FC) method graph of 2, 4-DBAF Polymer

Table: 6. Study of Kinetic Profiles and Thermodynamic Variables of the Polymer System

Polymer	Activation KJ mol^{-1} (Freeman-	Energy[Ea] (Sharp-Wentworth)	Entropy Change (ΔS), (J)	Free energy change(ΔF), KJ	Frequency Factor (Z) Sec^{-1}	Apparent Entropy change	Order of reaction

	Carroll)					**(S*)**	**(n)**
2, 4-DBAF	25.3	27.39	-210.71	107.57	546	-60.29	0.9

The thermodynamic parameters associated with the thermal decomposition of the 2,4-DBAF copolymer namely Gibbs free energy change (ΔF)**,** entropy change (ΔS)**,** apparent entropy change (S*)**,** and the frequency factor (Z)were calculated and are summarized in Table 6**.** The activation energy (Ea) values obtained from both the (FC) and (SW) methods showed close agreement, confirming the consistency and reliability of the kinetic evaluations. A notably low frequency factor (Z) suggested, thermal phase of decay of the 2, 4-DBAF polymer resin proceeds through a relatively slow reaction mechanism**.** Furthermore, the negative entropy change (ΔS) indicates that the transition state is more ordered than the initial state, implying a more structured arrangement of the copolymer in the activated complex compared to the reactants.

A detailed comparison of the activation energy values for different phase of decay, obtained using both methods, is provided in Table 7, further supporting the thermal stability profile of the 2, 4-DBAF polymer.

Table: 7. Analysis of Activation Energy (Ea) Associated with the Decomposition of 2,4-DBAF Polymer

Polymer	Stages	Temp. variation	Functional group depletion	Weight reduction (%)	Activation (Ea)(KJ/mol) (SW)	Activation (Ea)(KJ/mol) (FC)
2,4-DBAF polymer	1th	40.0-150	H_2O molecule entrapped	3.29	85.03	25.38
2,4-DBAF polymer	2nd	150-320	degradation two -OH groups	36.70	28.99	28.39
2,4-DBAF polymer	3th	320-480	Reduction of phenyl ring along with two -CH_2 groups	59.20	12.18	12.31
2,4-DBAF polymer	4th	480-710	Loss of acrylamide moiety.	85.03	86.16	86.02

Conclusion

In this study, a novel polymer was successfully synthesized and thoroughly characterized. The existence of chemically active sites within the prepared resins made them effective for eliminating toxic metal ions from water-based solutions. The resins exhibited good porous nature and major surface area, which contributed to their enhanced metal ion uptake, as confirmed through batch adsorption studies. Among the tested metal ions, the polymer demonstrated superior adsorption

efficiency for Co^{2+} and Cd^{2+}, suggesting strong selectivity. Thermogravimetric analysis (TGA) revealed that the synthesized polymer exhibits excellent thermal stability, which has vital applications in elevated-temperature manufacturing effluent practice, wastewater purification, stain industries, and even as a fireproof material. The kinetic parameters derived among both the (SW) and (F-C) methods showed good agreement, indicating a common degradation mechanism. Additionally, the low value of the frequency factor (Z) implies a sluggish thermal degradation process of the polymer, with kinetic data aligning with second-order or higher-order reaction pathways. Overall, the synthesized polymer resin holds significant promise as a thermally stable, constructive, and reusable adsorbent in favour of withdraw of toxic cation ions from contaminated environments.

Acknowledgement

The authors gratefully acknowledge the Principal of Taywade College, Mahadula, Koradi, Nagpur, India, for their continuous reinforcement and motivation throughout the process of this work. Special thanks are also extended to Prof. W. B. Gurnule, Head, Department of Chemistry, Kamla Nehru Mahavidyalaya, Nagpur, for his invaluable guidance, assistance, and motivation during the research.

REFERENCES

1. W. B. Gurnule, R. U. Rathod, A. D. Belsare and N. C. Das, Mat. Tod. Proc, 2020; 29:1044.
2. W. B. Gurnule, H. D. Juneja, L. J. Paliwal, Rev, & Fun. Polym, 2002; 50:95-100.
3. W. B. Gurnule, P. K. Rahangdale, L. J. Paliwal, R. B. Kharat, Rev. Fun. Polym, 2003; 55: 255-265.
4. W. B. Gurnule, H. D. Juneja, L. J. Paliwal, In. J. Chem, 2000; 39: 1110-1113.
5. W. B. Gurnule, P. K. Rahangdale, L. J. Paliwal, R. B. Kharat, Synth React Inorg Met Org Chem 2003; 33: 1187.
6. N. Sidharaj, G. Rajarajan, M. Senthil, Mater. Today Proc. 2021; 42: 1030– 1036.
7. S. S. Rahangadale, W. B. Gurnule, Desali. Wat. Tret, 2015; 55:1506-1815.
8. Y. U. Rathod, V. Pandit, D. Bhagat, W. B Gurnule, Mat. Tod. Proc, 2022; 53: 123-129.
9. R. N. Singru, W. B. Gurnule, V. A. Khati, A. B. Zade, J. R. Dontulwar, 2010;263:200-210.
10. El-shazly R, Kamal R, Nassar A, Ahmed N, Sayed G, Appl. Petro. Res, 2020; 10: 115.
11. W. B. Gurnule, Y. U. Rathod, A. D. Belsare, N. C Das, Mat. Tod. Proc, 2020; 15:611.
12. W. B. Gurnule, N. C Das, K. V Vajpai, Y.U. Rathod, Mat. Tod. Proc 2020; 29: 1071-1076.
13. S. P. Chakole, Y. U. Rathod, V. U. Pandit, Mat. Tod. Proc, 2022; 52: 96.
14. W. B. Gurnule, P. K. Gupta, R. H. Gupta, Y. U. Rathod, N. B. Singh,.Int. Conf. Ener. Tech, 2023; 1281: 012026.
15. P. G. Gupta, R. H. Gupta, W. B. Gurnule, S. N. Rao, Y. U. Rathod, Mat. Sci, 2023; 30: 838-844.
16. S. S. Rahangdale, W. B. Gurnule, Mat. Tod. Proc, 2020; 43:163-174.

17. Y. U. Rathod, S. B. Zanje, W. B. Gurnule, J. Phy Conf Ser, 2021; 1913: 012061.
18. N. Sidharaj, G. Rajaran , M. Senthil, Mat. Tod. Proc 2020; 42: 1030-1036.
19. W. B. Gurnule, R. R. Dubey, D. S. Bhagat, Y. U. Rathod, B. P. Kafle, J. Mod Nanotechnol, 2022; 2: 10.
20. M. B. Thakre, W. B. Gurnule, Mat. Tod. Proc. 2019; 3: 516–525.
21. J. V. Khobragade, M. Ahamed, W. B. Gurnule, synthesis and characterization of copolymer resin derived from pthallic acid and melamine. J. Chem. Pharm. Res, 2014; 6:364.
22. W. B. Gurnule, N.C. Das, Mat. Tod. Proc. 2019; 15: 611–619.
23. S. S. Rahangdale, N. C. Das, K. Vajpai, W.B. Gurnule, Int. J. Recent Sci. Res 2019; 10: 31772–31778.
24. W. B. Gurnule, Y. U. Rathod, and A. D. Belsare, Mat. Tod. Proc, 2020; 29: 1044-1049.
25. N. C. Das, W. B. Gurnule, Int. J. Curr. Eng. Sci. Res 2019; 6: 1414–1425.
26. C. Kohad, W. B. Gurnule, Mat. Today Proc 2019; 15: 438–446.
27. W. B. Gurnule, R. U. Rathod, A. D. Belsare, N. C. Das, Mat. Tod. Proc, 2020; 29:1044.
28. S. Morsch, Y. Liu, S.B .Lyon, S. R. Gibbon, B. Gabbriele, M. Malanin, K. Eichhorn, Polym. Degrad. Stabil. 2020; 176.
29. S. Chinaglia, M. Tosin, F. Polym. Degrad. Stabil 2020; 147: 237–244.
30. S. S. Rahangdale, W. B Gurnule, J. Appl. Polym. Sci, 2018; 43: 108-120.
31. S. Barkade, P. Bansod, V. Doss, S. Mardikar, Adv. Sci. Engg. Medic 2020; 12: 198-206.
32. N. C. Das, Y. U. Rathod, V. Pandit, W. B. Gurnule, Mat. Tod. Proc 2020; 53: 80-85.
33. M. M. Rangari, S. S. Rahangdale, S. Shrivastva, Y. U Rathod, Indian. J. Engr. Mat. Sci, 2023; 30: 816-822.
34. R. H. Gupta, P. Gupta, W. B. Gurnule, Int. J. Chem. Conf. 2019; 6: 101-107.
35. P. Gupta, R. H. Gupta, W. B. Gurnule, Resin-IV: Appl. Polym. Sci 2020; 8: 156-162.
36. S. P. Chakole, K. Nandekar, W. B. Gurnule, J. Phys. Conf. Ser 2021; 1913: 1–8.
37. W. B. Gurnule, S. P Chakole, N.C Das, Mat. Tod. Proc, 2020; 63: 1125-1136.
38. W. B. Gurnule, C.G Kohand, Res. J. Pharm. Bio. Chem. Sci, 2018; 9: 393-402.
39. Y. U. Rathod, W. B. Gurnule. Mat. Tod. Proc 2020; 6: 163-170.
40. W. B. Gurnule, C.G. Kohand, Res. J. Pharm. Bio. Chem. Sci, 2018; 9: 393-402.
41. S. K. Mandavgade, W. B. Gurnule, Mat. Tod. Proc. 2022; 60: 1814-1818.
42. V. R. Bisen, W. B. Gurnule, Int. J. Curr. Eng. Sci. Res. 2019; 6: 1309–1316.